The Astronomical Journal, 137:3533–3540, 2009 March doi:10.1088/0004-6256/137/3/3533
© 2009. The American Astronomical Society. All rights reserved. Printed in the U.S.A.

ENVIRONMENTS OF QSOs AT REDSHIFT 0.9–1.3*

J. B. Hutchings[1], P. Scholz[1], and L. Bianchi[2]
[1] Herzberg Institute of Astrophysics, 5071 West Saanich Road, Victoria, B.C. V9E 2E7, Canada; john.hutchings@nrc.ca
[2] Department of Physics and Astronomy, Johns Hopkins University, 3400 North Charles Street, Baltimore, MD 21218, USA
Received 2008 August 7; accepted 2008 December 21; published 2009 February 17

ABSTRACT

We analyze new deep *g*- and *i*-band imaging of 16 QSOs in the redshift range 0.9–1.3 with the Canada–France–Hawaii Telescope. The principal points of interest are the symmetry and signs of tidal effects in the QSO hosts and nearby (companion) galaxies. The sample measures are compared with similar measures on randomly selected field galaxy samples. Asymmetry measures are made for all objects to $g \sim 22$, and magnitudes of all galaxies 2 mag fainter. The QSOs are found in denser environments than the field, and are somewhat offset from the centroid of their surrounding galaxies. The QSO hosts appear more disturbed than other galaxies. While the QSO companions and field galaxies have the same average asymmetry, the distribution of asymmetry values is different. QSO companions within 15″ are fainter than average field galaxies. We discuss scenarios that are consistent with these and other measured quantities.

Key words: galaxies: evolution – galaxies: interactions – quasars: general

1. INTRODUCTION AND OBSERVATIONS

Imaging studies of QSOs have ranged from the local universe to those at redshift near to 6. From these and related studies, it is widely accepted that nuclear activity arises from accretion episodes on to massive central black holes in galaxies, and there are many scenarios for the process. Given the evidence for the connections between galaxy stellar properties and the central black hole mass, there is interest in studying QSO episodes in galaxies, at all redshifts, for clues as to how the black hole and galaxies develop this connection (e.g., Salviander et al. 2007). At low redshifts, there is considerable evidence that QSO host galaxies have had recent merging of tidal disturbance events, which activate the nuclear accretion process. At redshifts 2 and higher, host galaxies appear to be in their early stages of assembly, with high star formation. Thus, these probably represent different stages in the evolution of both galaxy and central black hole.

There are few environmental studies of QSOs at redshifts near 1. Falomo et al. (2004) and Kotilainen et al. (2007) discuss samples at redshift 1.2 and higher, while Kukula et al. (2001) investigated a sample of nine, with redshift 0.8–1.0. There are several investigations at redshifts 2 and somewhat higher (e.g., Ridgway et al. 2001; Hutchings et al. 2002). Most of these investigations were done at NIR wavelengths, where the contrast with the nucleus is expected to be better, and where ground-based AO works best. The main focus of these papers is the nature of the host galaxy, and there is some consensus that radio-loud objects have higher luminosity hosts, but many are luminous elliptical-type galaxies. Lacy (2006) gives a good summary of the work on higher redshift QSOs to that date.

The redshift range around 1 is when large galaxies are assembled, and may be in the process of forming the disk structures common in the present epoch. This work describes an investigation of QSO host galaxies and environments to learn more about this stage of their evolution, based on a new and relatively bias-free sample. Our resolution and wavelength range are not optimized for host galaxy details, and the main focus of this paper is galaxies that may be associated with the QSOs, and their morphology. In particular, we are interested in the asymmetry of such galaxies (and QSO hosts), which can be characterized by deviations from elliptical contours with radius, even if small-scale details are not well resolved. We are particularly interested in asymmetry of the fainter outer parts of galaxies, which arise from recent merging and tidal events among them. Few QSO studies in this redshift range have discussed this aspect. Wold et al. (2001) discuss the galaxy environments of QSOs at redshift 0.5–0.8 in a general way. Hutchings & Proulx (2008) discuss companion galaxy asymmetries in a low-redshift sample, and this paper is a similar investigation near redshift 1.

The sample is derived from the combined Sloan Digital Sky Survey (SDSS) and *Galaxy Evolution Explorer* (*GALEX*) surveys, which overlap in the shallow and medium *GALEX* surveys (see, e.g., Bianchi et al. 2007). Initial samples of some 3000 and 14,000 objects, respectively, were drawn from two-color planes such as FUV–NUV versus NUV–*r*, in the locations where QSOs separate out from stars and galaxies (see Bianchi et al. 2005; Bianchi 2008). Within these is a subsample of about 700 objects identified as QSOs by their SDSS spectra. We selected those in the redshift range 0.9–1.3, and declination 10°–40°, for imaging with the Canada–France–Hawaii Telescope (CFHT). Observations were made of 16 of these with the Megaprime camera of the CFHT. This sample is thus a subset of those investigated by Bianchi et al. (2007), which have photometric coverage from 1500 Å to 9000 Å.

The observations consist of images with *g* and *i* filters, of exposure 400 and 500 s, respectively, carried out between 2006 October and 2007 January. At least two exposures were taken in each filter, and several had more. Image quality was in the range 0.″6–1.″2 FWHM for most of the observations. Table 1 summarizes the QSOs observed. The QSO absolute magnitudes are in the range −24 to −26 in *g* band, which is in the middle of the range for QSO luminosities. At the redshift of the QSOs, the observations are sampling rest-band wavelengths of about 2400 Å and 3800 Å. The FIRST radio catalog does not cover the part of the sky where the sample is, so we do not know if any are radio-loud.

* Based on observations obtained with the Canada–France–Hawaii Telescope, which is operated by CNRS of France, NRC of Canada, and the University of Hawaii.

Table 1
Cataloged SDSS and *GALEX* Properties of Sample Objects

R.A.	Decl.	E_{B-V}	FUV	NUV	u	g	r	i	z	Redshift
00 32 59	15 49 59	0.056	22.14	20.76	20.03	19.78	19.51	19.60	19.23	0.98
00 33 50	15 46 14	0.057	23.37	21.26	20.25	20.28	20.01	19.96	20.13	1.26
00 36 34	14 35 46	0.093	20.39	19.61	19.66	19.41	19.07	19.02	18.83	1.01
00 41 59	14 54 47	0.091	22.16	20.52	19.94	19.79	19.35	19.21	19.25	1.18
00 44 41	15 38 50	0.048	20.99	19.94	19.44	19.23	19.12	19.17	19.04	0.93
00 45 46	15 50 24	0.050	21.39	19.59	19.61	19.54	19.16	19.18	19.13	1.16
00 46 14	15 38 36	0.056	22.43	21.06	20.53	20.46	20.86	19.97	19.52	1.16
00 46 36	16 01 30	0.059	20.51	19.52	19.10	18.91	18.63	18.60	18.69	1.12
00 54 44	14 46 46	0.054	19.65	18.36	18.19	17.93	17.78	17.80	17.60	0.91
01 17 44	14 50 11	0.056	21.02	20.05	19.93	19.63	19.26	19.10	19.12	1.07
01 22 46	14 32 03	0.042	21.60	20.93	20.69	20.47	20.32	20.14	20.41	1.19
01 22 54	14 51 03	0.054	19.65	18.71	18.68	18.74	18.42	18.37	18.30	1.23
01 23 00	15 11 48	0.059	20.27	19.34	18.75	18.69	18.38	18.33	18.44	1.28
01 23 06	15 39 10	0.083	21.62	20.35	20.10	19.96	19.53	19.36	19.56	1.07
01 24 44	13 26 42	0.039	21.29	19.73	19.01	18.71	18.47	18.38	18.53	1.26
01 47 27	14 21 51	0.050	20.15	18.93	18.36	18.27	18.09	18.09	18.00	1.03

2. MEASUREMENTS

The QSOs were first identified on each CFHT image. They are located at the same spot among the 36 CCDs, about 12″ from the edge of one. This means there is a gap of about 11″ of sky on this side of each QSO. We identified and made measurements of all galaxies within 75″ (400 pixels) of the QSO, with exceptions where they lie close to bright stars or image flaws. Several stars were also selected and measured to characterize the point-spread functions (PSFs) in each image. For each object and the QSO itself, the flux and position were recorded using the "imexamine" task of IRAF.

For all except the faintest galaxies, the "ellipse" task was used to fit contours at a fixed set of radii increasing uniformly on a log scale. For each contour, an asymmetry index is calculated as (Contour level)$^{1.5}$ × (sum of the absolute values of the third harmonic deviations from an ellipse) × (semimajor axis)$^{1.5}$. This quantity is slightly different (has a different signal level exponent) from that used by Hutchings & Proulx (2008), but is less dependent on the total signal so that objects of widely different flux as well as size can be compared. As in Hutchings & Proulx (2008), the weighting also is designed to be sensitive to faint outer asymmetries that are signatures of tidal events, which otherwise would be overwhelmed by small asymmetries (such as dust lanes or disk arms or nuclear saturation) seen in the bright inner contours. Plots of this index with contour radius show where the asymmetries lie within each image. A mean asymmetry index is the mean of the individual contour asymmetry values lying between radii 4 pixels (about the resolution limit of the observations), and where the signal lies less than 10% above the sky value. This mean is normalized by the total signal from the object, so that galaxies of different brightness can be compared. Hutchings & Proulx (2008) discuss other tests and properties of this index.

The images of the faintest galaxies were too noisy for ellipse fitting, but we have recorded their position and flux, down to 3000 counts in each image. We used the SDSS magnitudes from Table 1 to calibrate the images, and this limit corresponds to $g < 24.1$ and $i < 24.4$. The asymmetry measures were derived for galaxies to about 1.5 mag brighter than these values. Galaxies overall brighter than the related QSOs are considered to be foreground objects and were not measured. In general, all individual exposure images were measured, as well as combined images, for each filter and for both filters combined. Combined images were constructed by shifting and adding, so as to eliminate flaws and cosmic ray events, as well as increase signal to noise. In a few cases, single-pixel cosmic rays were edited out by hand, where they were affecting the asymmetry measurements. In all cases, accurate sky subtraction was important, and great care was taken with this. Fluxes determined by "imexam" and "ellipse" were compared, since they involve independent estimates of the sky level, and had to agree within 10% for the flux to be adopted as final. In the case of faint objects that were not fitted with ellipse, both imexam and subarray pixel statistics around the objects were used for this comparison. Where this agreement was not obtained, the sky levels were adjusted until they did.

We made all the same measurements in control fields, for comparison with the QSO fields. These were centered on positions within the same CCD as the QSO, lying more than 2′ from the QSO and at least 400 pixels of the CCD edge. The positions within this roughly 4′ × 9′ area of sky were selected by a random number generator. Where there were multiple exposures of QSOs, the same control objects were used. Table 2 gives average asymmetry values for different object classes. We discuss details in subsequent sections.

Figure 1 shows the distribution of image quality, by star FWHM values. The nonintegral bin values arise from using pixels as the units of measure. The figure also shows the values for the QSOs. While very similar, the QSO distribution is skewed to higher values, which suggests they are marginally extended compared with the stars, although the formal comparison of the distributions shows only 20% probability that they are different.

3. BIASES AND GALAXY COUNTS

Before looking for trends and differences between subsamples, we need to look at possible biases in the data set. The obvious ones to check are image quality, photometric calibration, and dependence on redshift and magnitude of objects.

Figure 2 shows the photometric calibration, based on the SDSS g and i magnitudes, and the mean fluxes for them from our data. Zero points have been applied to each color in the plots. The scatter increases for fainter objects, but in QSOs there is always some possibility of real variability at the level of a few tenths of a magnitude, between the observation epochs.

Table 2
Asymmetry Measurements

Type	Mean Asymmetry	Mean *g+i* Asymmetry	Mean *g* Asymmetry	Mean *i* Asymmetry	Number of Objects
QSOs[a]	0.010[b]	0.008	0.008	0.012	16
Stars[c]	0.005		0.006	0.004	30
Galaxies (QSO Field)	0.024	0.023	0.023	0.026	94
Control Galaxies	0.027	0.024	0.028	0.029	136
QSO Galx <200 pixel	0.031	0.026	0.033	0.034	34
Control Galx <200 pixel	0.023	0.022	0.025	0.024	33

Notes.
[a] QSO host values (nucleus removed) ∼5 times higher than these values.
[b] Does not include *g+i* measurements.
[c] Median, matched to QSO magnitudes.

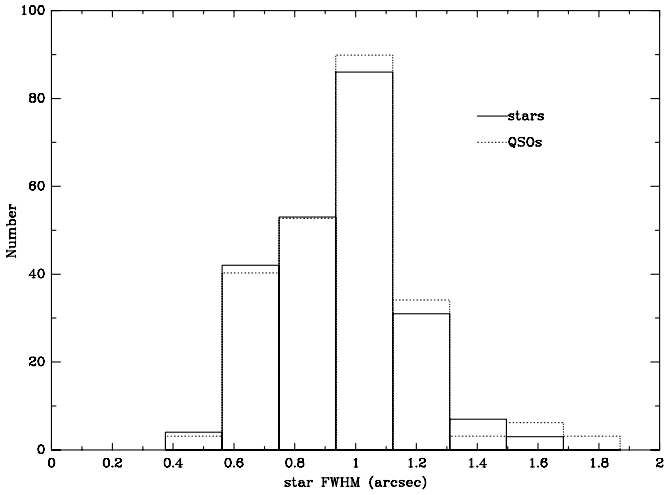

Figure 1. Distribution of FWHM for stars in the data, compared with those for QSOs, scaled to the same total.

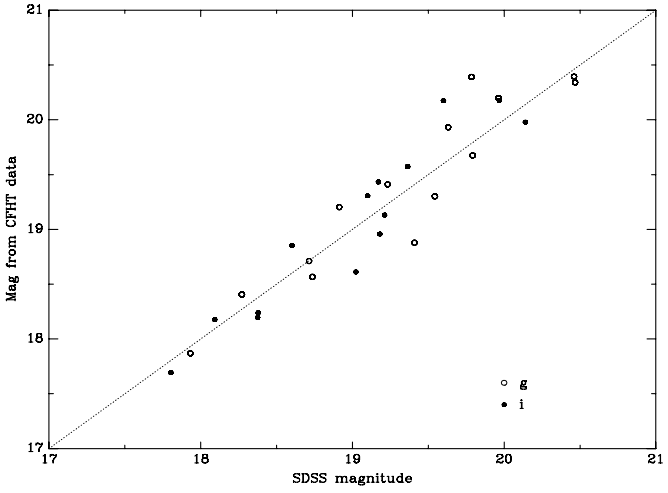

Figure 2. Photometric calibration based on SDSS magnitudes and our mean fluxes for our data on individual QSOs.

Figure 3 shows some illustrative plots. They show that there is little or no dependence of the asymmetry value with redshift, signal level, or image quality. A few of the stars have high asymmetries in good image quality, which we ignore as due to flaws or faint blends. The lowest asymmetry values are not seen in the faintest stars, but these values are lower than any seen in QSOs or galaxies, and the value is robust over a factor of

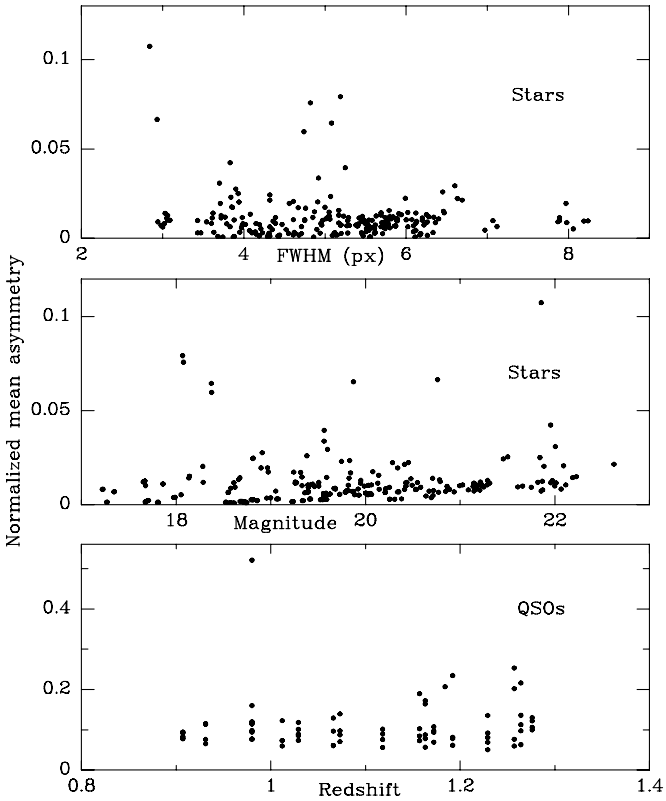

Figure 3. Looking for asymmetry-measure biases with image quality, brightness, and redshift. The asymmetry measurements have no significant correlation with these quantities.

100 signal range of all QSOs and galaxies in our program. The redshift range is relatively small and no trend is seen among the individual QSO measures.

Because the QSOs were situated close to a CCD edge, and hence a gap in sky coverage, it is necessary to correct the galaxy counts for the missing area of sky. The gap amounts to approximately 10% of the total area investigated. The way we made the correction was to reflect the galaxies an equal distance from the QSO on the other side of the gap, into the gap, and use these for statistics on galaxy properties with distance from the QSO. Figure 4 shows the stacked distribution of all the galaxies measured, for all QSOs and all control fields. In the QSO distribution, the gap lies between +12″ and +23″ from the QSO.

Figure 5 shows the sky density of galaxies around the QSOs and in the control fields. The lower plots are galaxies with

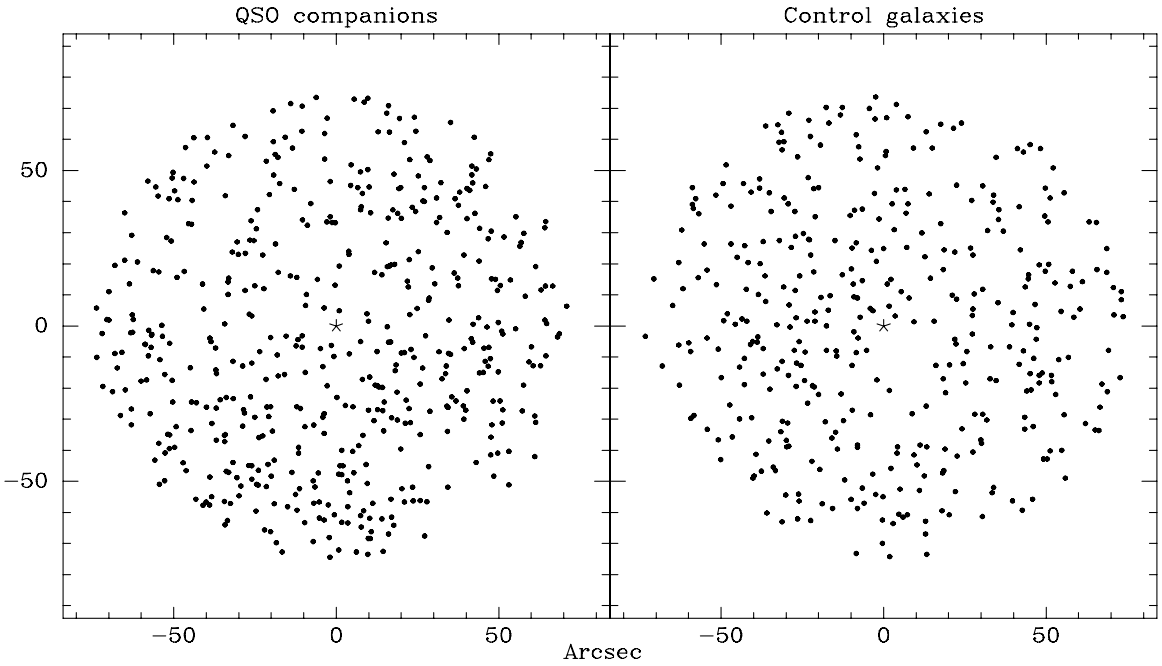

Figure 4. Spatial distribution of all galaxies measured around the QSOs and for randomly selected (control) positions far from the QSO.

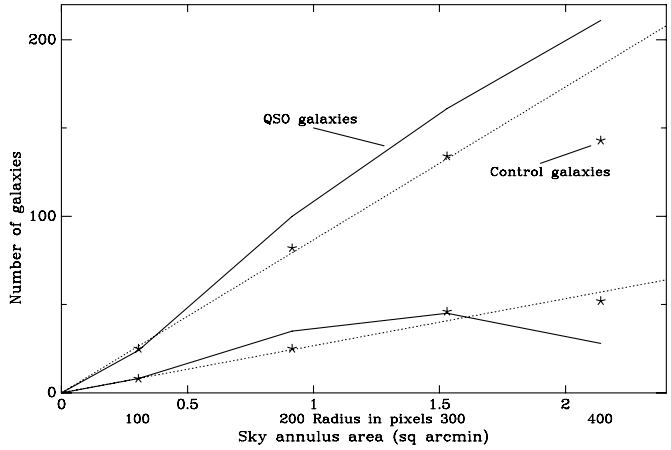

Figure 5. Galaxy counts per unit area of sky, for the QSOs and control fields. Uniform density should yield linear plots. Linear fits (dotted lines) are shown for the control field galaxy counts. The upper plots include all galaxies to our flux limit, and the lower plots are those which had asymmetry measurements on them. The ratio of total to asymmetry-measured galaxies is about 3 (see the text discussion).

asymmetry measures and the upper plots include all the fainter galaxies to the limits mentioned above. For an even sky density, the plots should form straight lines. The dotted lines are those corresponding to the control fields. It appears that the QSOs lie in regions of greater galaxy density, especially in the radius range 30″–50″ (150–270 pixels). Both sets appear to suffer from some incompleteness in the largest radius bin. Within the areas covered, the QSO fields have 28% more galaxies, and within 1′ they are 17% higher. The QSO measurable companion galaxies are 14% more numerous within 1′. The QSO fields thus overall have an excess of order 25% over the foreground and background galaxy counts in our sample. This needs to be taken into account in looking for differences between the QSO and field galaxy environments.

The ratio of total galaxies down to our faint flux limit, to ellipse-measured galaxies is close to 3 (see Figure 5), but with considerable scatter. Galaxy counts show trends with QSO redshift, varying by a factor of 2 over the redshift range 0.9–1.3, with higher total counts in the lower redshift cases. While there is considerable scatter, this suggests that there are real groups of galaxies associated with the QSOs, and we are seeing a flux limit effect with redshift. However, the scatter does not warrant any more detailed conclusion.

It is of interest to see if the QSOs are centrally placed with respect to their surrounding galaxies. The offset between mean position of all surrounding galaxies, and the QSO, should become smaller with increasing projected distance from the QSO, if their positions are random and unconnected with the QSO. If the QSO is centrally placed within a real group, this offset will be small for all projected distances. These offsets for the control fields do indeed decrease with increasing sky radius, as expected for random control field origins. The QSO offsets, however, become systematically larger with increasing radius to our radius limit of just over 1′. This is consistent with an associated set of real companions, among which the QSOs are offset by an average of about 5″. The overall mean offset of companions for all QSOs, is the same as for the control groups, which is consistent with the individual QSO offsets being in random directions, among our sample fields.

4. PHOTOMETRY

Figure 6 shows the magnitudes of galaxies in approximately 10″ annuli around the QSOs, compared with the same for the randomly placed control positions. We have plotted both mean and median values, as they differ somewhat due to the nongaussian distribution of magnitudes. The magnitudes themselves are from the combined *g*- and *i*-band images, for maximum signal on the fainter ones. The standard deviations of the means are typically 1 mag, but for the innermost radius bins, they are about 0.5 mag. As expected, the magnitudes in the control fields show no trend with position. However, the QSO fields have fainter galaxies in the inner bins, and brighter galaxies in the middle-range bins, which is where the galaxy

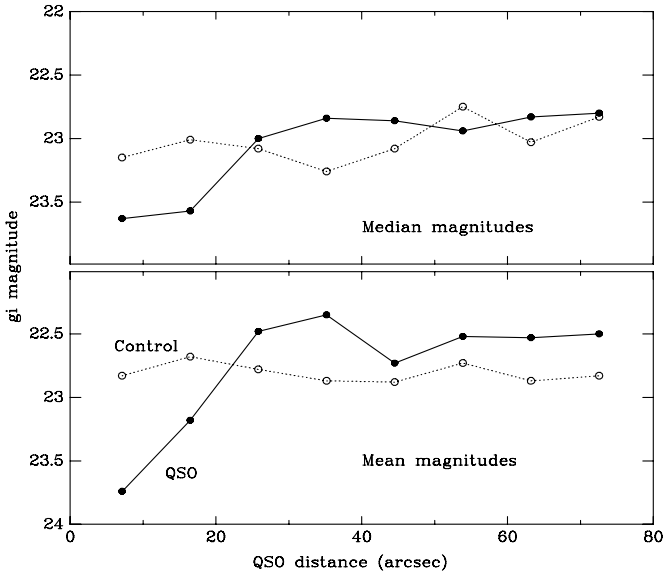

Figure 6. Magnitude trends with projected distance from the QSOs compared with field values. Points are all galaxies within the given radius from the QSO or random control origin position.

count excess is found. The suggestion is that the QSO-associated galaxies are faint by some 0.5 mag near to the QSO and the excess galaxies at 30″–50″ radii are brighter than field galaxies by a few tenths of a magnitude.

We may compare the $g-i$ colors of galaxies from our data. The control field galaxies and the QSO companions have mean and median $g-i$ colors close to 0.93 for both groups. The companions in the 25″–50″ distance range also have this color, so there are no large mean color differences between these populations. But the QSO companions have fewer blue galaxies and fewer red galaxies than the field—the color range is much less spread, and formally the two distributions are different at the 96% level. This indicates a more uniform population, among the QSO companions, with none in star formation and fewer old galaxies. Bearing in mind that ∼80% of the galaxies are foreground or background (from the 25% excess in the QSO fields, as noted in the previous section), this indicates a very different population among the true QSO companions. The QSO colors are much bluer, with an average value of 0.34.

Figure 7 shows the seven filter magnitudes from *GALEX* and SDSS, for all the sample. The Lyman break lies between the FUV and NUV for this redshift range, and Lyα lies in the NUV band. The distribution is much the same for all individual objects in the sample. We compare these with similar average magnitudes for normal QSOs at other redshift (Bianchi et al. 2009), with the bands shifted to bring them all to redshift about 1.1. While the filter bandpasses do not match exactly the same rest wavelengths in these comparisons, there appears to be little difference between them. The low-redshift sample has lower luminosity, and hence presumably lower Lyα flux, and possibly some host galaxy light, which would account for the relatively fainter NUV and u magnitudes for these. The sample in this paper does not show the extreme UV characteristics discussed by Bianchi et al. (2009). The SDSS spectra cover the rest wavelength range from C III 1909 to Hγ, and are not significantly different from the spread of SDSS spectra for randomly selected QSOs in this redshift range.

Looking in more detail at the photometry, the NUV–i index shows a trend of increasing with redshift, with two exceptions. The exceptions make the overall trend nonsignificant, but it is what is expected as the Lyman absorption moves into the NUV bandpass. The FUV–NUV index shows a lot of scatter and no significant trend with redshift. The FUV and NUV magnitudes show no correlations with redshift, and do correlate well with the SDSS magnitudes. This shows up in individual plots of the format of Figure 7, as most lines connecting dots for individual QSOs do not cross each other. There are nominal values of foreground reddening based on the lines of sight from the extinction maps of Schlegel et al. (1998), but the values are small and show no correlation with FUV magnitude or $g-r$ index. Thus, we expect that extinction plays no significant role in the sample.

5. ASYMMETRY IN GALAXIES

Individual mean asymmetry values on the same object agree to within 10%, with an average spread about half of this. The i-band images show higher asymmetry than the g band. For QSOs the asymmetry in i band is 29% higher than in g band (which drops to 15% if we ignore three high outliers). For galaxies the i-band asymmetry excess is 14%, while for stars it is only 5%. Thus, while the i-band images may be slightly more intrinsically asymmetric, there seems to be a real difference in the galaxies, in the same sense. In addition, the mean asymmetry (g and i combined) is higher for blue galaxies—both QSO companions and field galaxies. The median asymmetry rises by 50% as $g-i$ goes from 1.75 to 0.25 and the mean value rises by 32%, for all galaxies. Galaxies that are blue are more asymmetric, but the asymmetry is more apparent in redder light. This may arise from a combination of star formation and dust, for instance. There is no significant change with UV-optical color: this also may be a result of dust, which has greater extinction in the UV. As a "sanity check" we noted galaxies that appeared on inspection to be interacting or disturbed. These galaxies on average had measured asymmetry indices 2–3 times that for the others.

Figure 8 shows the mean values of the asymmetry indices for the different classes of object. The first point to note is that the QSO companion galaxies and the field galaxy sample have essentially the same mean asymmetry. Thus, there is no gross difference in morphology. The value for stars is lower, confirming that we are resolving and measuring the galaxy morphology. Star values contain some high outliers, probably due to faint galaxies or structures within the PSF, so we have derived a median value for bright stars, matching the QSO magnitudes, for comparison with the QSO asymmetries. The distributions of asymmetry values for galaxies and QSOs are well spread about their means and their median values are essentially the same. The distribution of asymmetry values for QSOs and matched magnitude stars are different at the 98% level, by the S-Z test, so that the QSO asymmetries are not simply the effect of the nuclear PSF.

Thus, while the QSOs are dominated by their unresolved nuclei, and have low asymmetry values, as seen in Table 2, we can attempt to estimate the asymmetries of the host galaxies. The average absolute magnitude of the QSO nuclei is a factor of 20 brighter than L*, so to estimate their host galaxy asymmetries, we have renormalized the QSO values by a (conservative) constant factor of 10, after subtracting the median asymmetry for bright stars (0.005), which is the lowest asymmetry that can apply to any of our objects. The QSO magnitudes are increased in Figure 8 by the same factor of 10 (2.5 mag) to approximate the host galaxy magnitudes. The host galaxy asymmetries, derived

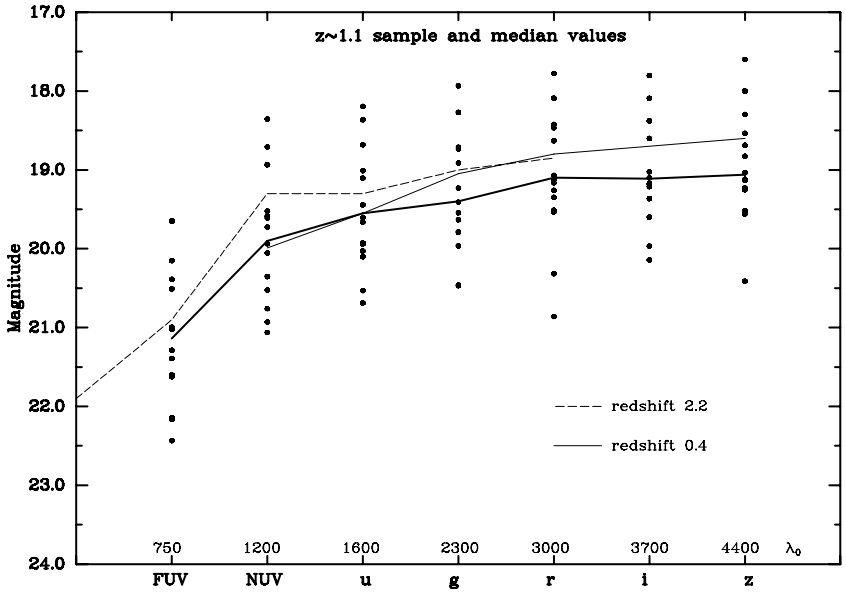

Figure 7. *GALEX* and SDSS magnitudes for the sample QSOs (dots), with the median values connected by the thick line. The lighter lines represent medians from samples at different redshifts, with bandpass bins shifted to match the $z \sim 1$ sample observations.

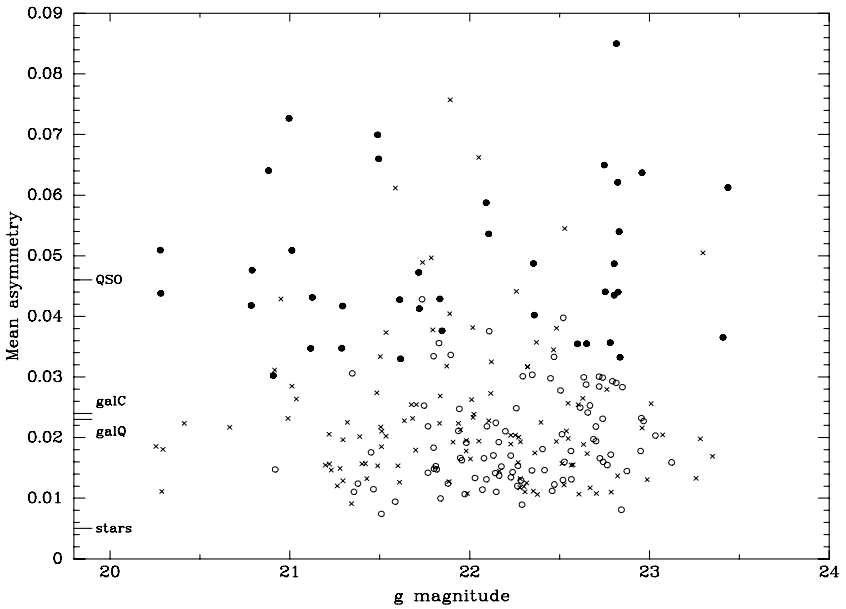

Figure 8. Mean normalized asymmetry for various objects as a function of magnitude. Filled dots are QSOs, open circles their companions, and crosses the field galaxies. The QSO asymmetry values above the star value have been multiplied by a factor of 10 to derive the values for the host galaxies, and compare with the other galaxies. The QSO host galaxy magnitudes have accordingly been increased by 2.5 from the QSOs, for the same reason. To avoid crowding the diagram, star values are not plotted, but their median is shown at the edge of the box.

this way, are higher than the nonhost galaxies (Figure 8), and this signal presumably lies in the faint outer parts of the images. As an independent approach, we note the FWHM values for the QSO images are on average 2% larger than the stars, with a total spread from 97% to 109% of the star values from the same images.

Figure 9 shows the asymmetry as a function of distance from the QSO (and random sky points for field galaxies). There is no obvious trend with projected distance from the QSO, or, as already noted in Figure 8, overall difference from the field galaxies. However, we have sketched in lines that suggest a higher asymmetry population, and a lower asymmetry population for the QSO companions, and a single dashed line for the field galaxies. Bearing in mind that there are projection effects and line-of-sight contaminants, the plot is consistent with companion galaxies that have higher asymmetries near the QSO, and perhaps also some that have lower than normal asymmetry. From Figure 8, the low asymmetry galaxies are faint. Possibly we are seeing galaxies that are disturbed and some that have been stripped, as a result of being in a group environment.

Figure 10 shows the distributions of QSO and field galaxy asymmetry values of combined *g* and *i* images. The field galaxies are overall skewed to higher values than the QSO galaxies, except for the highest values. This difference is more marked in *i* than *g*-band data. A Kolmogorov–Smirnov (K–S) test indicates that the distributions in Figure 10 are different at the 98% confidence level. In all sets of filter images, the difference is significant at over 90%. If we look only at the galaxies within

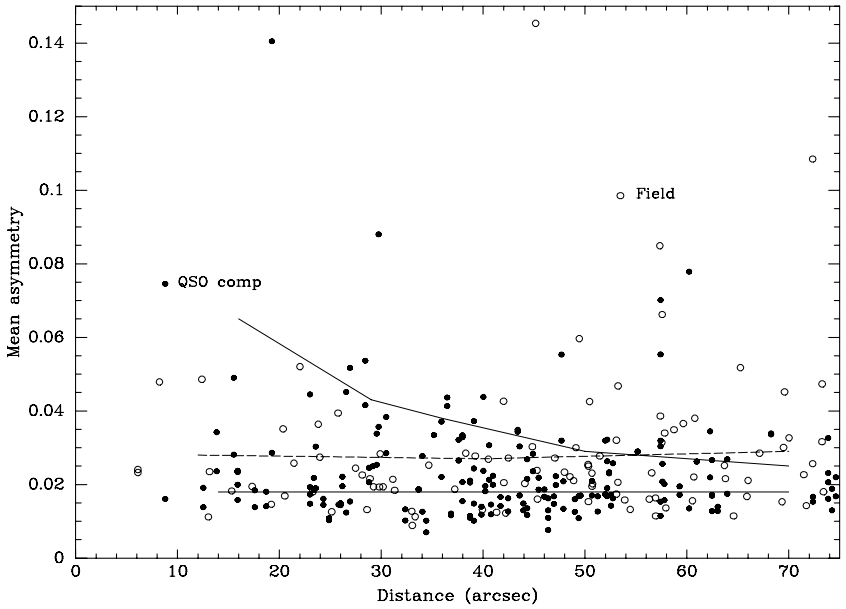

Figure 9. Galaxy asymmetry with projected distance from the QSO (dots), and for field galaxies about random origin (circles). The dashed line shows the mean value for field galaxies and the two solid lines sketch in two possible distributions for the QSO companions, as discussed in the text.

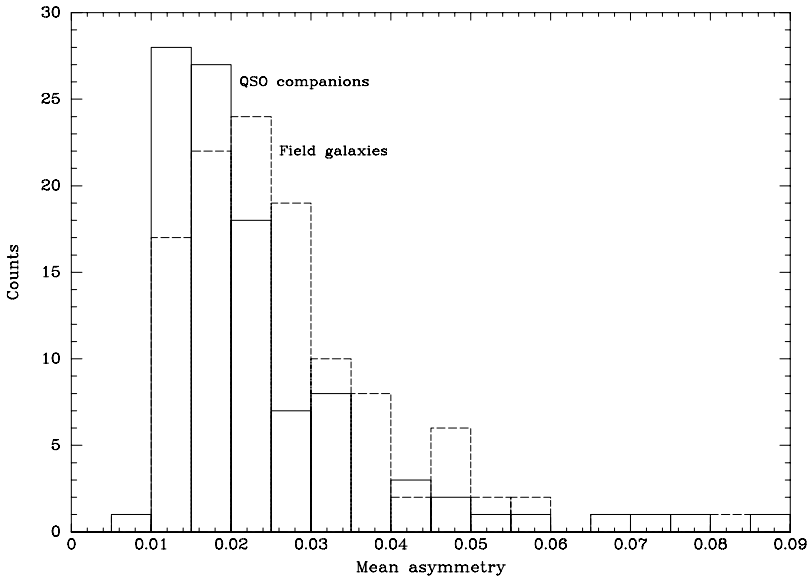

Figure 10. Distributions of asymmetry index for QSO companions (solid line) and field galaxies (dashed line). The distributions are different at the 98% confidence level.

35″ of the QSO, the double-peaked distribution of the QSO companion asymmetries is more marked, as can be seen in Figure 9. The K–S test actually gives lower probability for this kind of difference, since the field galaxies have a single-peaked broader distribution of asymmetries. We note that the faintest galaxies have no asymmetry measures, so we are unable to examine this property of the faint galaxies that lie closest to the QSOs (see Figure 6).

6. SUMMARY AND DISCUSSION

The sample of QSOs we have investigated appear to be normal in their luminosities and spectral energy distributions, and lie in the redshift range 0.9–1.3, which is not well investigated for QSO environments. The data set is uniform and has an average resolution of 0.″9. The QSOs are marginally resolved with the data.

The photometric calibration is good to a few tenths of a magnitude, and there are no systematics with image quality, magnitude, and QSO redshift within the ranges present. Control fields in the same data have been used extensively to enable good comparison with the QSO environments.

The QSOs are on average not centrally located with their surrounding galaxies, down to about 24 mag. The QSOs appear to live in significantly denser environments than random places in the sky. The QSO companion galaxies have significantly different color distribution from the field, having less spread in color. The QSO environments have significantly fainter galaxies within ∼15″ than the field. The galaxies investigated in the QSO environments are estimated to contain about 75% nonassociated line-of-sight galaxies in the range of brightness measured.

Making an average correction for the nuclear point source, the host galaxies are about two times more asymmetric than the

companion or field galaxies in the same range of luminosity. The companion and field galaxies have about twice the asymmetry as stars in the fields. The companion galaxies do not have the same asymmetry distribution as field galaxies, having more symmetrical and more asymmetrical ones, in a double-peaked distribution. The more asymmetrical galaxies lie within 30″ of the QSO.

The picture that emerges for this sample is that the QSOs have asymmetrical structure, as do their closer bright companion galaxies in compact groups of diameter some 600 kpc. In the innermost 100 kpc, the companion galaxies are fainter than the average field galaxies, and there are also several galaxies with higher than normal symmetry.

This is consistent with interactions within the groups, some of which triggered the QSO event. The number of faint and symmetrical galaxies might indicate a population of postinteraction stripped galaxies with little star formation. The brighter asymmetrical galaxies are bluer and have higher asymmetry, indicating ongoing or recent interaction events.

The excess galaxies in the QSO fields (see Figure 5) are 1.9 within 90 kpc, 3.8 within 280 kpc, and 7.5 within 365 kpc, average per QSO. These numbers are similar to the excess galaxies found at $z \sim 0.3$ by Hutchings & Proulx (2008). However, the absolute magnitude of the galaxies in this sample has a faint limit about 1 mag more luminous than those in the low-redshift sample. *K* corrections may reduce that, but this is still a high density of galaxies, in which interactions must be common. We note that the excess is not seen within 100 kpc of the QSO, so it may be that the QSO is clearing out the central part of the group, perhaps by merging.

Our data indicate that QSOs at redshift near 1 live in dense small groups of galaxies, in which merging and tidal interaction are occurring frequently, and that the QSOs themselves are affecting the galaxies closest to them, either by merging or by the QSO radiation, since there are fewer and fainter galaxies close to the QSOs. It would clearly be of interest to obtain high-resolution deep imaging of these QSO fields, to test this scenario and gather essential details of the galaxy morphology.

We thank the CFHT QSO team for making the observations, and a referee for helping to improve our presentation.

REFERENCES

Bianchi, L. 2008, in Space Astronomy: the UV Window to the Universe, APSS (Berlin: Springer)
Bianchi, L., Hutchings, J. B., Efremova, B., Herald, J. E., Bressan, A., & Martin, C. 2009, AJ, in press
Bianchi, L., et al. 2005, ApJ, 619, L27
Bianchi, L., et al. 2007, ApJS, 173, 659
Falomo, R., Kotilainen, J. K., Pagani, C., Scarpa, R., & Treves, A. 2004, ApJ, 604, 495
Hutchings, J. B., Frenette, D., Hanisch, R., Mo, J., Dumont, P. J., Redding, D. C., & Neff, S. G. 2002, AJ, 123, 2936
Hutchings, J. B., & Proulx, C. 2008, AJ, 135, 1692
Kotilainen, J. K., Falomo, R., Labita, M., Treves, A., & Uslenghi, M. 2007, ApJ, 660, 1039
Kukula, M. J., Dunlop, J. S., McLure, R. J., Miller, R., Percival, W. J., Baum, S. A., & O'Dea, C. P. 2001, MNRAS, 326, 1533
Lacy, M. 2006, Astrophysics Update 2, arXiv:astro-ph/0601255
Ridgway, S. E., Heckman, T. M., Calzetti, D., & Lehnert, M. 2001, ApJ, 550, 122
Salviander, S., Shields, G. A., Gebhardt, K., & Bonning, E. W. 2007, ApJ, 662, 131
Schlegel, D. J., Finkbeiner, D. P., & Davis, M. 1998, ApJ, 500, 525
Wold, M., Lacy, M., Lilje, P. B., & Serjeant, S. 2001, in QSO Hosts and Their Environments, ed. I. Márquez et al. (Dordrecht: Kluwer), 33